frontiers in Energy Research

BRIEF RESEARCH REPORT
published: 24 June 2020
doi: 10.3389/fenrg.2020.00109

Three-Dimensional Carbon-Supported MoS_2 With Sulfur Defects as Oxygen Electrodes for Li-O_2 Batteries

Yun Liu[1], Yipeng Zang[1], Xinmiao Liu[1], Jinyan Cai[1], Zheng Lu[1], Shuwen Niu[1], Zhibin Pei[2], Teng Zhai[3] and Gongming Wang[1]**

[1] *Hefei National Laboratory for Physical Sciences at the Microscale, Department of Chemistry, University of Science & Technology of China, Hefei, China,* [2] *School of Environment and Energy, South China University of Technology, Guangzhou, China,* [3] *School of Materials Science and Engineering, Nanjing University of Science and Technology, Nanjing, China*

Recently, Li-O_2 batteries have been considered to be promising next-generation energy storage devices owing to their high theoretical specific energy. However, due to the sluggish reaction kinetics of oxygen conversion, practical applications cannot achieve the desired results. By introducing vacancies in the MoS_2 basal plane and using an *in-situ* synthesis method, we demonstrated the excellent catalysis of MoS_{2-x} for oxygen redox kinetics, which can improve Li-O_2 battery performance. The prepared MoS_{2-x} displays little polarization, with a potential gap of 0.59 V and a high discharge capacity of 8,851 mA h g^{-1} at a current density of 500 mA g^{-1}. The improved performance is mainly attributable to abundant S defects and plentiful diffusion channels in the MoS_{2-x}/carbon 3D structural cathodes, which enable the adsorption of gaseous oxygen, reaction intermediates, and discharge products. To the best of our knowledge, these structures fabricated through 3D network design and surface modulation are among the best oxygen conversion catalysts developed so far, offering a new vista for the design of Li-O_2 catalysts and beyond.

Keywords: MoS_{2-x}, defects, catalytic sites, cathode, Li-O_2 battery

OPEN ACCESS

Edited by:
Jun Yan,
Harbin Engineering University, China

Reviewed by:
Liang Huang,
Huazhong University of Science and Technology, China
Xu Xiao,
Drexel University, United States

****Correspondence:***
Zhibin Pei
peizb@scut.edu.cn
Gongming Wang
wanggm@ustc.edu.cn

Specialty section:
This article was submitted to Electrochemical Energy Conversion and Storage, a section of the journal Frontiers in Energy Research

Received: *21 April 2020*
Accepted: *11 May 2020*
Published: *24 June 2020*

Citation:
Liu Y, Zang Y, Liu X, Cai J, Lu Z, Niu S, Pei Z, Zhai T and Wang G (2020) Three-Dimensional Carbon-Supported MoS_2 With Sulfur Defects as Oxygen Electrodes for Li-O_2 Batteries. Front. Energy Res. 8:109. doi: 10.3389/fenrg.2020.00109

INTRODUCTION

Rechargeable non-aqueous Li-O_2 batteries, which have an ultra-high theoretical energy density (>3,450 Wh Kg^{-1}), have been widely studied as a promising alternative energy storage system for the next generation of long-range electric vehicles and other high-energy devices (Cheng and Chen, 2012; Zhang P. et al., 2018; Zhang X. et al., 2018). Although the operation of Li-O_2 batteries is based on a simple electrochemical reaction ($2Li^+ + O_2 + 2e^- > Li_2O_2$, $E_0 = 2.96$ V), on the cathode, where there is a triple-phase contact interface, much more complicated *in-situ* reactions occur consisting of an oxygen reduction reaction (ORR) and an oxygen evolution reaction (OER) (Xu et al., 2016; Lyu et al., 2017). During discharge, ORR has been generally accepted to occur in two major steps. Firstly, O_2 is reduced to O_2^-, followed by combination with Li^+ to form LiO_2. Then, these superoxide intermediates undergo further electrochemical reduction or chemical disproportionation to form Li_2O_2, which is deposited on the cathode (Aurbach et al., 2016; Dong et al., 2018; Chaozhu et al., 2019). The charge process (OER) is far more complicated since the mechanism is indistinct and there are multiple charging intermediates, such as $Li_{2-x}O_2$, LiO_2, and

O_2^- (Li and Chen, 2017; Lim et al., 2017). Many researchers have demonstrated that the bonding ability of the reaction intermediates to the solid (Li_2O_2)-solid (catalyst) interface is a key factor governing OER activity in the presence of a catalyst (Lu et al., 2013; Zhu et al., 2015; Lai et al., 2018). In general, a series of reactions starting from the adsorption of gaseous oxygen place great demands on the active sites on the cathode surface, while simultaneously, the deposition of a large amount of insulating Li_2O_2 also requires that the cathode structure provide sufficient accommodation space (Liu et al., 2015; Feng et al., 2016). These sluggish and unsustainable reactions on the triple-phase contact interface of the cathode always result in poor round-trip efficiency, limited rate capacity, and weak durability, which are critical defects for Li-O_2 batteries, severely hindering their practical application. Thus, designing catalysts with high activity and a porous structure to promote kinetics reaction is a prerequisite for further advancement of Li-O_2 technology (Chang et al., 2017; Hu X. et al., 2017; Wu et al., 2017).

Until now, numerous studies have been devoted to exploring alternative electrocatalysts and designing a good cathode architecture as the main strategies for improving the kinetics of oxygen conversion. Among them, molybdenum disulfide (MoS_2) has outstanding performance and low cost as a star catalyst (Asadi et al., 2016, 2018; Behranginia et al., 2016). However, as a typical layered transition metal dichalcogenide, its reactivity is mainly attributable to the low-coordinated unsaturated fringe zone of the layered structure, and yet the predominantly highly exposed basal plane atoms have not yet exerted their unique structural advantages (Jaramillo et al., 2007). In the field of electrochemical catalysis and Li-S batteries, a lot of research has focused on increasing the number of edge active sites and modifying the basal plane to further optimize its activity (Li et al., 2011; Kibsgaard et al., 2012; Xie et al., 2013; Yin et al., 2016; Hu J. et al., 2017). For instance, through introducing edge defect sites and doping oxygen to increase chaos, Xie et al. promoted the transfer of plane electrons to the edge to enhance their electrochemical reactivity (Xie et al., 2013; Xie J. et al., 2013). Lin et al. found that MoS_{2-x}/rGO with defective sites can effectively catalyze the conversion of lithium polysulfide and accelerate its oxidation-reduction reaction kinetics. Defects such as MoS_2 edge sites and terrace surfaces have exhibited great electrochemical activity for the deposition of discharge products (Lin et al., 2017). Thus, surface regulation of MoS_2 to improve intrinsic conductivity and the number of active sites exposed on the basal plane could greatly improve catalysis activity, especially in Li-O_2 systems that have high requirements on the adsorption of active sites.

To essentially manipulate the intrinsic properties of MoS_2 to further enhance its application value for cathode catalysis, as well as to study the effect of S defects on MoS_2 activity in Li-O_2 batteries, we prepared sulfur-deficient MoS_2 nanoflakes (MoS_{2-x}) growing *in-situ* on macroporous carbon paper as the binder-free Li-O_2 battery cathode. The 3D hierarchical porous cathode structure not only provides excellent electrical conductivity but also facilitates efficient gas transportation and lithium-ion diffusion and accommodates a large number of discharge products to increase battery capacity. Impressively, in the presence of the S defects in MoS_{2-x} on porous carbon paper, the cathode exhibits excellent oxygen redox catalytic performance, with an overall potential gap of 0.59 V and a discharge capacity of 8,851 mA h g^{-1}. Scanning electron microscopy (SEM) images obtained after discharge also show the different Li_2O_2 morphologies formed on MoS_2 and MoS_{2-x}, which relate to the adsorption of intermediates onto their surface. To the best of knowledge, this performance makes MoS_{2-x} as one of the best oxygen conversion catalysts, and these methods of surface modulation could offer a new vista for the design of Li-O_2 catalysts and beyond.

EXPERIMENTAL DETAILS

Material Synthesis

In a typical procedure, 0.196 g ammonium molybdate [$(NH_4)_6Mo_7O_{24}{\cdot}4H_2O$] and 3.92 g sodium thiosulfate ($Na_2S_2O_3$) were dissolved in 18 mL deionized water with ultrasonic assistance. Then, the solution was transferred into a 20-mL Teflon-lined stainless-steel autoclave with punched carbon paper with a diameter of 11 mm as the growth substrate. After keeping the hydrothermal reaction temperature at 200°C for 20 h, the carbon paper was taken out, cleaned with deionized water and ethanol, and dried in a vacuum oven at 60°C for 10 h. MoS_2 growing on carbon paper was obtained at a loading of 0.8–1.0 mg. The MoS_{2-x} sample was formed by heating the prepared MoS_2 in a 10% H_2/Ar atmosphere at 500°C for 3 h.

Structural Characterization

The morphologies were characterized by scanning electron microscopy (SEM, JEOL-JSM-6700F), transmission electron microscopy (TEM, Hitachi H7650), and high-angle annular dark-field scanning TEM (HAADF-STEM, JEOL JEM-ARF200F TEM/STEM). X-ray diffraction (XRD) measurement was conducted on a Philips X'pert Super diffractometer with Cu Kα, λ =1.54178 Å, and Raman spectra were recorded on a Renishaw RM 3000 Micro-Raman system. X-ray photoelectron spectroscopy (XPS, ESCALAB 250 spectrometer, Perkin-Elmer) was collected at the BL10B of the National Synchrotron Radiation Laboratory (NSRL). The surface area and pore distribution plots were collected by Brunauer–Emmett–Teller (BET, Micromeritics ASAP 2020).

Electrochemical Measurements

The Li-O_2 electrochemical performance was measured in 2,032 cells with 19 pores on the steel cathode shells. All of the cells are assembled in an Ar-filled glove box (O_2, H_2O < 1 ppm) by using a lithium metal foil as the anode, a glass fiber separator as the separator, the prepared electrode as the gas cathode, and 75 vol% dimethyl sulfoxide (DMSO) and 25 vol% 1-ethyl-3-methylimidazolium tetrafluoroborate (EMIM-BF4) with 0.1 M lithium bis(trifluoromethanesulfonyl)imide (LiTFSI) (>99.0%) as the electrolyte. The cathode prepared by the coating method was made from a powder slurry of the corresponding material. The powdered samples were mixed with acetylene black and poly (vinylidene difluoride) (PVDF) in an 8:1:1 ratio, and commercial CNT samples were mixed with PVDF at 9:1 in

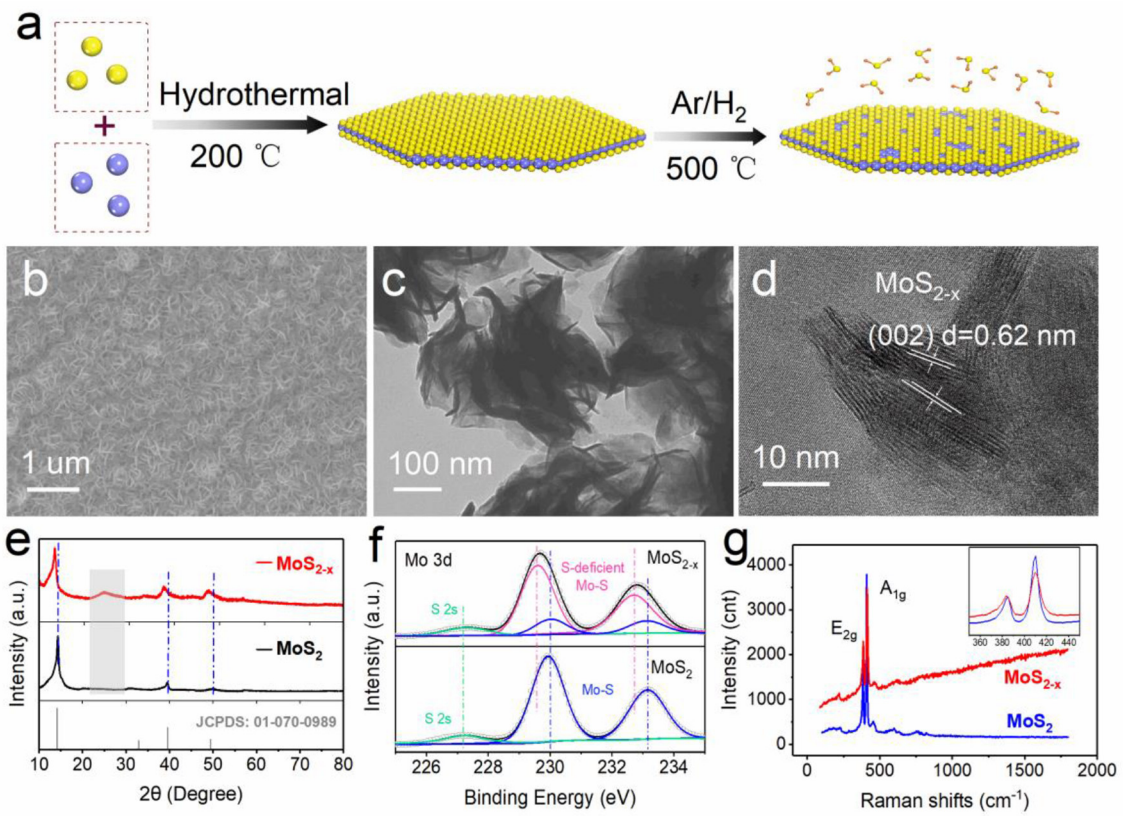

FIGURE 1 | Material synthesis and characterization. **(a)** Schematic of the synthesis. **(b)** SEM image of MoS_{2-x} on carbon paper. **(c)** TEM image of MoS_{2-x}. **(d)** High-resolution TEM of MoS_{2-x}. **(e)** XRD patterns of MoS_{2-x} and MoS_2. **(f)** XPS core-level Mo 3d spectra from MoS_{2-x} and MoS_2. **(g)** Raman spectra of MoS_{2-x} and MoS_2.

N-methyl-2-pyrrolidone (NMP). The coating slurry was then applied to the carbon paper with a loading of 0.7 mg. The electrochemical performances of the cathodes were tested using a specific capacity-controlled mode at various current densities in pure O_2. Electrochemical impedance spectroscopy (EIS) were performed under open-circuit voltage with the frequency ranging from 1 Hz to 100 kHz.

RESULTS AND DISCUSSION

Material and Structural Characterization

As shown schematically in **Figure 1a**, molybdenum source and sulfur source will nucleate and grow into flake-like MoS_2 crystals through hydrothermal reaction under high temperature and high pressure. When treated in an H_2/Ar atmosphere at high temperature, part of the sulfur will be taken away by the reducing atmosphere to form H_2S, leaving a lot of S defects on the MoS_2 basal plane. MoS_{2-x} with S defects shows more layers than do pristine MoS_2 nanoflakes and has larger surface area, as the SEM images in **Figure S1** show. It can also be seen from the TEM images in **Figure S2** that MoS_{2-x} has thinner nanoflakes at the edges, which may attribute to non-stoichiometric MoS_{2-x} with increased disorder of the atomic arrangement. It is these disordered S defects that endow the inert basal plane with a large amount of active sites at which to adsorb oxygen and discharge/charge intermediates and discretely induce the deposition of discharge products, promoting a series of oxygen redox catalytic processes. The SEM image in **Figure 1b** shows MoS_{2-x} nanoflakes uniformly and densely growing on carbon paper; this is enlarged in **Figure S3**. The TEM image and its enlarged view in **Figure 1c** and **Figure S4**, respectively, display the super-thin layer-like structure of MoS_{2-x} nanoflakes, which are about several nanometers thick. The high-resolution (HRTEM) image in **Figure 1d** reveals well-resolved lattice fringes with an interplanar spacing of 0.62 nm, which are assigned to the (002) plane of hexagonal MoS_2. We also performed HRTEM to characterize the defects of the MoS_{2-x} basal plane, as shown in **Figure S5**. The red regular hexagon indicates that the shooting angle is focused on the basal surface of hexagonal MoS_{2-x}. Many defects can be seen on the basal plane, as marked by the brown circle.

The effects of S defects on the structure of MoS_{2-x} were analyzed by XRD, and the results are seen in **Figure 1e**. The diffraction peaks of the MoS_2 nanoflakes can be well converted to No. 01-070-0989. For MoS_{2-x}, there was a slight shift to a lower degree, indicating an increase in the lattice spacing,

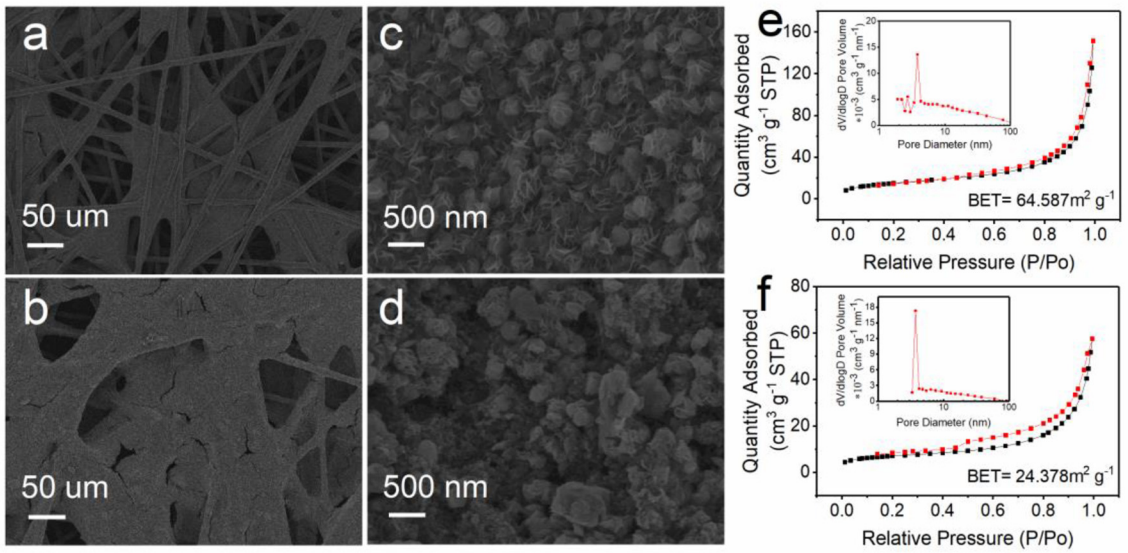

FIGURE 2 | Structural characterization of MoS_{2-x} growing on or coating carbon paper. **(a,b)** SEM images. **(c,d)** Enlarged SEM view of **(a,b)**. **(e,f)** Nitrogen adsorption and desorption isotherms and pore-size distribution.

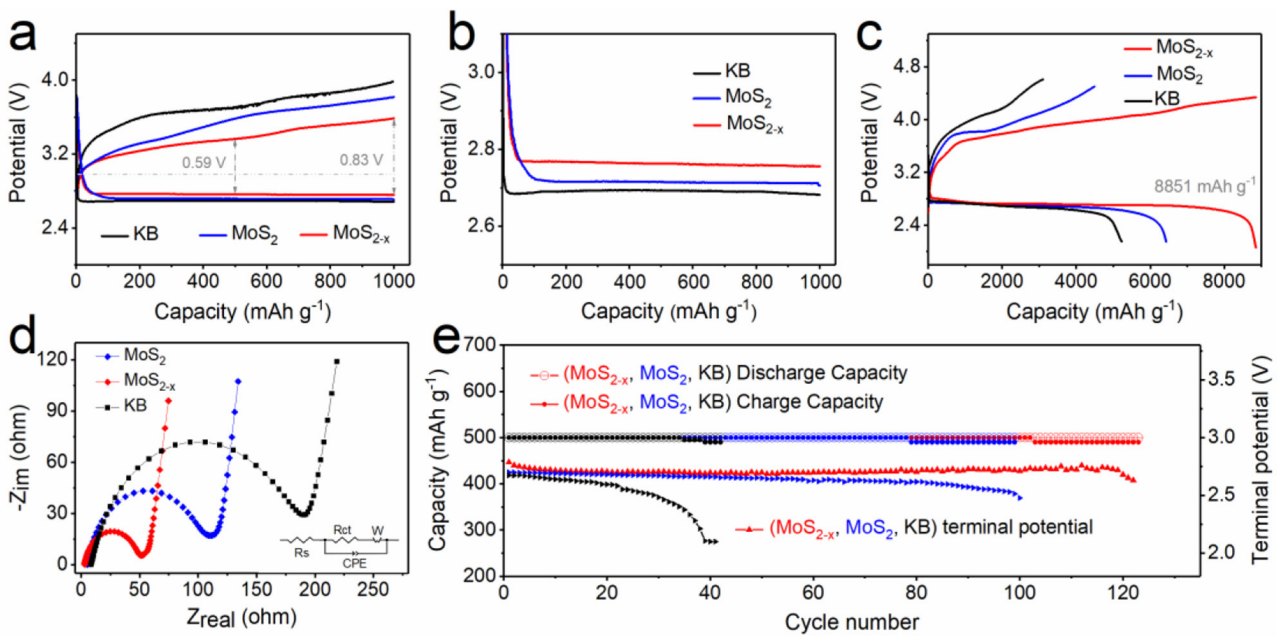

FIGURE 3 | Electrochemical properties. **(a)** First cycling galvanostatic discharge and recharge profiles of MoS_{2-x}, MoS_2, and Kejen Black. **(b)** Enlarged image of the discharge curves in **(a)**. **(c)** Full discharge and recharge curves of Li–O_2 batteries with MoS_{2-x} and MoS_2 cathodes. **(d)** EIS spectra of MoS_{2-x}, MoS_2, and Kejen Black at open-circuit voltages. The inset is the equivalent circuit. **(e)** Cycling stability and the terminal discharge potential of MoS_{2-x} and MoS_2 cathodes.

caused most likely by the removal of sulfur atoms. The resultant reduction of Mo, moving it to a lower oxidation state with a larger atomic radius, led to the increase in the lattice spacing. In addition, newly emerging diffraction peaks between 20 and 30 degrees represent the increase in the degree of disorder of the MoS_2 lattice. XPS analysis was conducted to obtain insights into the chemical composition and electronic states of MoS_{2-x} and MoS_2. **Figure 1f** displays the deconvoluted XPS Mo 3d spectra, in which MoS_{2-x} exhibits the characteristic peaks of both stoichiometric MoS_2 (blue) and sulfur-deficient MoS_2

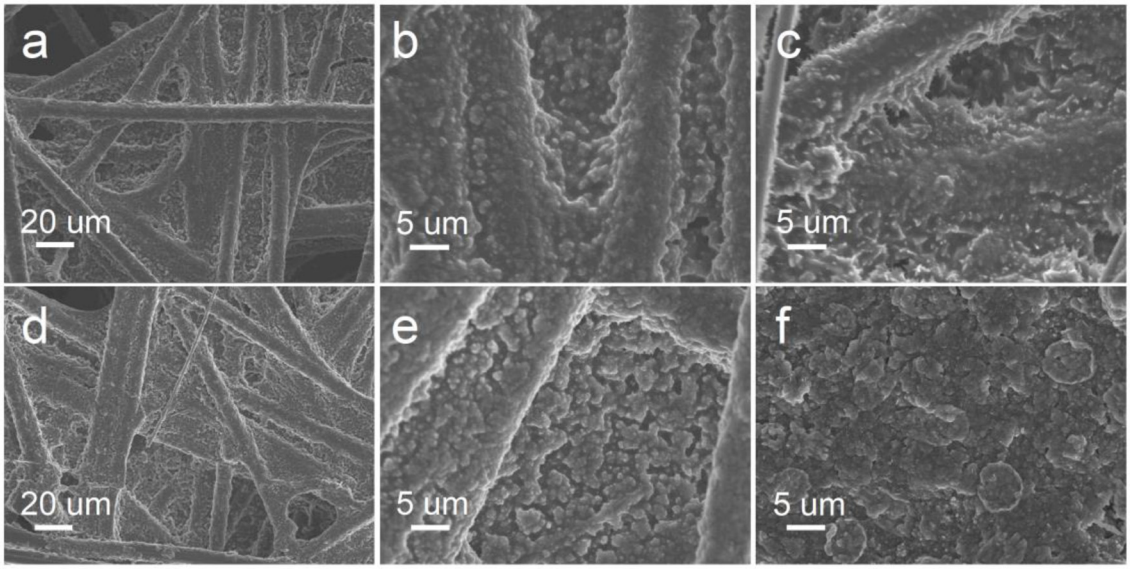

FIGURE 4 | Morphological evolution of the discharge products. **(a)** SEM image of MoS_{2-x} after discharge to 500 mA h g^{-1}. **(b)** Enlarged view of **(a)**. **(C)** SEM image of MoS_{2-x} after discharge to 1,000 mA h g^{-1}. **(d)** SEM image of MoS_2 after discharge to 500 mA h g^{-1}. **(e)** Enlarged view of **(d)**. **(f)** SEM image of MoS_2 after discharge to 1,000 mA h g^{-1}. Galvanostatic discharge with current at 500 mA g^{-1}.

(red). Specifically, the sulfur-deficient MoS_2 possesses lower binding energy than stoichiometric MoS_2 in Mo $3d_{5/2}$ (229.6 eV compared with 230.02 eV) and $3d_{3/2}$ (232.71 eV compared with 233.11 eV) doublets, illustrating the decrease in the valence state of Mo. Besides, the peak at 227.3 eV is attributed to S 2s, and the XPS total survey spectra and S 2p spectra are also displayed in **Figure S6**. In addition, the structural differences can also be detected by Raman spectroscopy. In **Figure 1g**, the fingerprint bands of MoS_2 are located at 376 and 402 cm^{-1}, caused by the in-plane (E_{2g}) and out-plane (A_{1g}) Mo-S phonon mode vibration of MoS_2, respectively. Obviously, the weakening of Raman peak intensity can be explained by the decrease in the content of vibration groups. The Raman peak is a statistical result, and the same peak broadening is due to lower structural uniformity of the vibrating molecules, which is caused by inducing S defects.

Considering the huge influence of the electrode structure on the performance of the battery, the loading methods of the catalyst MoS_{2-X} on porous carbon paper are also studied here. We compare a cathode of catalyst grown *in-situ* on carbon paper with a cathode coated with catalyst powder and find that the coated slurry easily blocked the original pores of the carbon paper and blocked the gas channel, as shown in **Figures 2a,b**; this can be compared with the pure carbon paper framework in **Figure S7**. Besides, the slurry used in the coating method will destroy the uniform arrangement of the catalyst on the conductive carbon paper, and the micron-level insulating binder used therein will also greatly affect the conductivity of the electrode, as shown in **Figures 2c,d**. N_2 adsorption–desorption techniques were employed to characterize the surface structural features. MoS_{2-x} (growing on carbon paper) exhibits a surface area of 64.587 m^2 g^{-1}, which is superior to the MoS_{2-x} coating on carbon paper (24.378 m^2 g^{-1}) and pure carbon paper (9.093 m^2 g^{-1}), as shown in **Figures 2e,f** and **Figure S8**. The isotherm profile in **Figure 2c** is categorized as type IV with a hysteresis loop (H3), and the pore-size distribution determined by the BJH shows pore diameters centered at a range of 4–30 nm (mainly mesopores). This meaningful 3D hierarchical porous structure not only acts as ion and gas transmission channels but also contributes to increasing the specific surface area to deliver more active sites and sufficient room to accommodate solid discharge products to achieve satisfying specific capacity performance.

Electrochemical Performance of Li-O_2 Batteries

To examine the electrochemical properties of the prepared MoS_{2-x} and MoS_2 cathodes, Kejen Black (denoted as KB) was employed as a comparison, and Li-O_2 2032 coin cells were assembled. At a current of 500 mA g^{-1} and a cutoff capacity of 1,000 mA h g^{-1}, the discharge and charge potential gap of MoS_{2-x} is 0.59 V, much lower than that of MoS_2 (0.87 V) and Kejen Black (1.03 V) at half capacity, as shown in **Figure 3a**. During the charge process, the charge potential platform of MoS_{2-x} is 3.55 V and the overpotential is 0.57 V, which is significantly lower than for MoS_2 (3.79, 0.81 V) and Kejen Black (3.96, 0.98 V), indicating excellent OER catalytic activity. For the discharge (ORR) process, as is enlarged in **Figure 3b**, MoS_{2-x} displayed a discharge platform at 2.75 V, higher than MoS_2 (2.71 V) and Kejen Black (2.68 V). Compared with the cathode constructed by the coating method, both MoS_{2-x} and MoS_2 have far superior performance in reducing

overpotential, demonstrating the structural advantages of a self-growing cathode for Li-O_2 batteries, as shown in **Figure S9**. The corresponding round-trip efficiency based on calculus is 85.56% for MoS_{2-x}, much higher than the values of 76.46, 76.61, 74.85, and 71.9% obtained for MoS_2 growing on carbon paper, MoS_{2-x}, MoS_2, and Kejen Black coating on carbon paper, respectively, as shown in **Figure S10**. Furthermore, to gain an insight into the full specific capacity of the MoS_{2-x} cathode, the MoS_{2-x} and MoS_2-based Li-O_2 batteries were tested under deep discharge/charge and limited capacity conditions. The MoS_2 cathode could deliver a high discharge capacity of about 6,312 mA h g^{-1} during the discharge process, while the charge process showed quite serious polarization and poor reversibility (**Figure 3c**). On the contrary, the MoS_{2-x} cathode could not only obtain a discharge capacity as high as 8,851 mA h g^{-1} but also exhibited better reversibility with lower charging energy. This improved performance can be attributed to it being a monolithic cathode with a hierarchical porous structure and extensive active deposition sites provided by S defects, which is vital for an O_2-based electrode in an energy storage device. We also performed extended galvanostatic discharge and charge tests with the current density varying from 200 to 2,000 mA g^{-1} to further assess the rate performance. The results are shown in **Figure S11**. The MoS_{2-x} cathode exhibits a small polarization with clear voltage plateaus and superior reversibility, demonstrating resistance to large currents and accelerated electrochemical reactions.

In addition, we conducted an EIS test at open-circuit voltage to study the interfacial kinetics in Li-O_2 batteries (**Figure 3d**), with the Nyquist plots fitted by an equivalent electrical circuit (**Figure 3d**, inset). MoS_{2-x} exhibits a lower charge-transfer resistance (Rct) of 50.8 Ω compared with MoS_2 (108.4 Ω) and Kejen Black (188.94 Ω), indicating that it has ultrafast charge transfer behavior. MoS_{2-x} achieves a lower energy barrier to trigger and support robust oxygen conversion and charge transfer, demonstrating a significant promotion of ORR and OER catalytic activity in Li-O_2 batteries. As shown in **Figure 3e**, the long cycling stability was tested at 500 mA g^{-1} with a cutoff capacity of 1,000 mA h g^{-1}. The terminal discharge potential of the MoS_2 cathode obviously decreases to 2.5 V after 99 cycles, while the battery with a MoS_{2-x} cathode can achieve more than 123 cycles before the terminal discharge potential reaches 2.6 V, displaying that it has superior reversibility and cycling stability. Based on the above results, we can conclude that the introduction of S defects greatly improves the cathode catalytic activity and capacity for Li-O_2 batteries.

Morphological Evolution of the Discharge Products

The morphologies of discharge products are accepted to be significant factors affecting the subsequent electrochemical reaction. Thus, SEM investigations were carried out to characterize the evolution of discharge products. After discharging to 500 mA g^{-1} for 1 h, the pores of the cathode were partially covered with film-like discharge products, as shown in **Figures 4a,b**. After continued discharge to 1,000 mA h g^{-1}, thicker aggregates were present on the MoS_{2-x} cathode (**Figure 4c**), indicating the continuous reduction of oxygen into discharge products and deposition on the cathode. For direct comparison, the typical morphologies of the MoS_2 cathode after discharging were also tested, as shown in **Figures 4d–f**. After discharging to 1,000 mA h g^{-1}, the cathode can be seen to be uniformly covered with patelloid products in **Figure 4c** and **Figure S12**, suggesting that the MoS_2 cathode behaves quite differences from the MoS_{2-x} cathode. During the discharging process, the exertion of a strong adsorption force on the intermediate discharge products always led the superoxide intermediate products to experience further electrochemical reduction, thus forming a film-like discharge product, while weak adsorption often led to large-sized crystal discharge products, which need higher energy for oxidative decomposition. On the surface of the MoS_{2-x} cathode, strong adsorption to discharge intermediates can be attributed to S defects, which enhance the adsorption activity and the number of adsorption sites and provide an excellent prerequisite for the subsequent charging process.

CONCLUSIONS

In summary, we have demonstrated that MoS_2 with S defects can intrinsically promote the corresponding thermodynamic and kinetic processes in Li-O_2 batteries. XRD and XPS are used to characterize the defects of the MoS_2 materials, which can act as active centers for the adsorption and conversion of superoxide intermediate products. SEM and BET tests demonstrate that *in-situ* growth on carbon paper can be used to successfully fabricate a multilayer hierarchical 3D structure that can provide abundant channels for ion and gas molecule diffusion. Due to these advantages, a MoS_{2-x} electrode exhibits an overpotential of 0.59 V and a discharge capacity of 8,851 mA h g^{-1} at a current density of 500 mA g^{-1}, showing the best performance. Moreover, the large number and film-like distribution of discharge products on the MoS_{2-x} surface means a stronger adsorption effect on intermediate products. Therefore, this study, in designing the 3D host materials and tuning the electronic structure of the MoS_2 surface, paves a new way to the high-energy application of Li-O_2 batteries.

DATA AVAILABILITY STATEMENT

The original contributions presented in the study are included in the article/**Supplementary Material**, further inquiries can be directed to the corresponding author/s.

AUTHOR CONTRIBUTIONS

GW and TZ designed and supervised the project. GW, ZP, and YL conducted the project and wrote and revised the manuscript. YZ conducted XPS measurements. XL helped to disassemble the batteries. ZL and SN performed SEM characterization and provided valuable help in the data analysis. All of the authors discussed the results and commented on the manuscript.

FUNDING

This work was supported by the National Key Research and Development Program of China (2017YFA0206703), the Natural Science Fund of China (Nos. 21771169, 11722543, and 11505187), the Fundamental Research Funds for the Central Universities (WK2060190074, WK2060190081, and WK2310000066), USTC start-up funding, and the Recruitment Program of Global Experts.

ACKNOWLEDGMENTS

We thank the Photoemission End stations at BL10B, the National Synchrotron Radiation Laboratory, for XPS characterizations.

SUPPLEMENTARY MATERIAL

The Supplementary Material for this article can be found online at: https://www.frontiersin.org/articles/10.3389/fenrg.2020.00109/full#supplementary-material

REFERENCES

Asadi, M., Kumar, B., Liu, C., Phillips, P., Yasaei, P., Behranginia, A., et al. (2016). Cathode based on molybdenum disulfide nanoflakes for lithium-oxygen batteries. *ACS Nano* 10, 2167–2175. doi: 10.1021/acsnano.5b06672

Asadi, M., Sayahpour, B., Abbasi, P., Ngo, A. T., Karis, K., Jokisaari, J. R., et al. (2018). A lithium-oxygen battery with a long cycle life in an air-like atmosphere. *Nature* 555, 502–507. doi: 10.1038/nature25984

Aurbach, D., McCloskey, B. D., Nazar, L. F., and Bruce, P. G. (2016). Advances in understanding mechanisms underpinning lithium-air batteries. *Nat. Energy* 1, 1–11. doi: 10.1038/nenergy.2016.128

Behranginia, A., Asadi, M., Liu, C., Yasaei, P., Kumar, B., Phillips, P., et al. (2016). Highly efficient hydrogen evolution reaction using crystalline layered three-dimensional molybdenum disulfides grown on graphene film. *Chem. Mater.* 28, 549–555. doi: 10.1021/acs.chemmater.5b03997

Chang, Z., Xu, J., and Zhang, X. (2017). Recent progress in electrocatalyst for Li-O_2 batteries. *Adv. Energy Mater.* 7:1700875. doi: 10.1002/aenm.201700875

Chaozhu, S., Jiazhao, W., Jianping, L., Hua-Kun, L., and Shi-Xue, D. (2019). Understanding the reaction chemistry during charging in aprotic lithium–oxygen batteries: existing problems and solutions. *Adv. Mater.* 31:1804587. doi: 10.1002/adma.201804587

Cheng, F., and Chen, J. (2012). Metal-air batteries: from oxygen reduction electrochemistry to cathode catalysts. *Chem. Soc. Rev.* 41, 2172–2192. doi: 10.1039/c1cs15228a

Dong, J.-C., Zhang, X.-G., Briega-Martos, V., Jin, X., Yang, J., Chen, S., et al. (2018). *In situ* Raman spectroscopic evidence for oxygen reduction reaction intermediates at platinum single-crystal surfaces. *Nat. Energy* 4, 60–67. doi: 10.1038/s41560-018-0292-z

Feng, N., He, P., and Zhou, H. (2016). Critical challenges in rechargeable aprotic Li-O_2 batteries. *Adv. Energy Mater.* 6:1502303. doi: 10.1002/aenm.201502303

Hu, J., Zhang, C., Jiang, L., Lin, H., An, Y., Zhou, D., et al. (2017). Nanohybridization of MoS2 with layered double hydroxides efficiently synergizes the hydrogen evolution in alkaline media. *Joule* 1, 383–393. doi: 10.1016/j.joule.2017.07.011

Hu, X., Wang, J., Li, Z., Wang, J., Gregory, D. H., and Chen, J. (2017). MCNTs@MnO_2 nanocomposite cathode integrated with soluble O_2-carrier co-salen in electrolyte for high-performance Li-air batteries. *Nano Lett.* 17, 2073–2078. doi: 10.1021/acs.nanolett.7b00203

Jaramillo, T. F., Jorgensen, K. P., Bonde, J., Nielsen, J. H., Horch, S., and Chorkendorff, I. (2007). Identification of active edge sites for electrochemical H_2 evolution from MoS2 nanocatalysts. *Science* 317, 100–102. doi: 10.1126/science.1141483

Kibsgaard, J., Chen, Z., Reinecke, B. N., and Jaramillo, T. F. (2012). Engineering the surface structure of MoS_2 to preferentially expose active edge sites for electrocatalysis. *Nat. Mater.* 11, 963–969. doi: 10.1038/nmat3439

Lai, N. C., Cong, G., Liang, Z., and Lu, Y. C. (2018). A highly active oxygen evolution catalyst for lithium-oxygen batteries enabled by high-surface-energy facets. *Joule* 2, 1511–1521. doi: 10.1016/j.joule.2018.04.009

Li, F., and Chen, J. (2017). Mechanistic evolution of aprotic lithium-oxygen batteries. *Adv. Energy Mater.* 7:1602934. doi: 10.1002/aenm.201602934

Li, Y., Wang, H., Xie, L., Liang, Y., Hong, G., and Dai, H. (2011). MoS2 nanoparticles grown on graphene: an advanced catalyst for the hydrogen evolution reaction. *J. Am. Chem. Soc.* 133, 7296–7299. doi: 10.1021/ja201269b

Lim, H. D., Lee, B., Bae, Y., Park, H., Ko, Y., Kim, H., et al. (2017). Reaction chemistry in rechargeable Li-O_2 batteries. *Chem. Soc. Rev.* 46, 2873–2888. doi: 10.1039/c6cs00929h

Lin, H., Yang, L., Jiang, X., Li, G., Zhang, T., Yao, Q., et al. (2017). Electrocatalysis of polysulfide conversion by sulfur-deficient MoS_2 nanoflakes for lithium–sulfur batteries. *Energy Environ. Sci.* 10, 1476–1486. doi: 10.1039/c7ee01047h

Liu, Q. C., Xu, J. J., Xu, D., and Zhang, X. B. (2015). Flexible lithium-oxygen battery based on a recoverable cathode. *Nat. Commun.* 6, 1–8. doi: 10.1038/ncomms8892

Lu, Y.-C., Gallant, B. M., Kwabi, D. G., Harding, J. R., Mitchell, R. R., Whittingham, M. S., et al. (2013). Lithium–oxygen batteries: bridging mechanistic understanding and battery performance. *Energy Environ. Sci.* 6, 750. doi: 10.1039/c3ee23966g

Lyu, Z., Zhou, Y., Dai, W., Cui, X., Lai, M., Wang, L., et al. (2017). Recent advances in understanding of the mechanism and control of Li_2O_2 formation in aprotic Li-O_2 batteries. *Chem. Soc. Rev.* 46, 6046–6072. doi: 10.1039/c7cs00255f

Wu, S., Qiao, Y., Yang, S., Ishida, M., He, P., and Zhou, H. (2017). Organic hydrogen peroxide-driven low charge potentials for high-performance lithium-oxygen batteries with carbon cathodes. *Nat. Commun.* 8, 1–9. doi: 10.1038/ncomms15607

Xie, J., Zhang, H., Li, S., Wang, R., Sun, X., Zhou, M., et al. (2013). Defect-rich MoS_2 ultrathin nanosheets with additional active edge sites for enhanced electrocatalytic hydrogen evolution. *Adv. Mater.* 25, 5807–5813. doi: 10.1002/adma.201302685

Xie, J. F., Zhang, J. J., Li, S., Grote, F., Zhang, X. D., Zhang, H., et al. (2013). Controllable disorder engineering in oxygen-incorporated MoS_2 ultrathin nanosheets for efficient hydrogen evolution. *J. Am. Chem. Soc.* 135, 17881–17888. doi: 10.1021/ja408329q

Xu, J. J., Chang, Z. W., Wang, Y., Liu, D. P., Zhang, Y., and Zhang, X. B. (2016). Cathode surface-induced, solvation-mediated, micrometer-sized Li_2O_2 cycling for Li-O_2 batteries. *Adv. Mater.* 28, 9620–9628. doi: 10.1002/adma.201603454

Yin, Y., Han, J., Zhang, Y., Zhang, X., Xu, P., Yuan, Q., et al. (2016). Contributions of phase, sulfur vacancies, and edges to the hydrogen evolution reaction catalytic activity of porous molybdenum disulfide nanosheets. *J. Am. Chem. Soc.* 138, 7965–7972. doi: 10.1021/jacs.6b03714

Zhang, P., Zhao, Y., and Zhang, X. (2018). Functional and stability orientation synthesis of materials and structures in aprotic Li-O_2 batteries. *Chem. Soc. Rev.* 47, 2921–3004. doi: 10.1039/c8cs00009c

Zhang, X., Mu, X., Yang, S., Wang, P., Guo, S., Han, M., et al. (2018). Research progress for the development of Li-air batteries: addressing parasitic reactions arising from air composition. *Energy Environ. Mater.* 1, 61–74. doi: 10.1002/eem2.12008

Zhu, J., Wang, F., Wang, B., Wang, Y., Liu, J., Zhang, W., et al. (2015). Surface acidity as descriptor of catalytic activity for oxygen evolution reaction in Li-O_2 Battery. *J. Am. Chem. Soc.* 137, 13572–13579. doi: 10.1021/jacs.5b07792

Conflict of Interest: The authors declare that the research was conducted in the absence of any commercial or financial relationships that could be construed as a potential conflict of interest.